Energy 47 (2012) 488–497

Contents lists available at SciVerse ScienceDirect

Energy

journal homepage: www.elsevier.com/locate/energy

A three-dimensional numerical modeling of thermoelectric device with consideration of coupling of temperature field and electric potential field

Xiao-Dong Wang [a,b,*], Yu-Xian Huang [c], Chin-Hsiang Cheng [d], David Ta-Wei Lin [e], Chung-Hao Kang [e]

[a] State Key Laboratory of Alternate Electrical Power System with Renewable Energy Sources, North China Electric Power University, Beijing 102206, China
[b] Beijing Key Laboratory of Multiphase Flow and Heat Transfer for Low Grade Energy, North China Electric Power University, Beijing 102206, China
[c] Department of Mechanical Engineering, National Chung Cheng University, Chiayi 62102, Taiwan
[d] Department of Aeronautics and Astronautics, National Cheng Kung University, Tainan 70101, Taiwan
[e] Institute of Mechatronic System Engineering, National University of Tainan, Tainan 700, Taiwan

ARTICLE INFO

Article history:
Received 12 May 2012
Received in revised form
28 August 2012
Accepted 9 September 2012
Available online 4 October 2012

Keywords:
Thermoelectric device
Numerical modeling
Coupling of temperature and electric potential
Variable properties
Convective boundary conditions

ABSTRACT

Thermoelectric devices (TEs) can achieve direct conversion of heat and electricity by semiconductor materials, coupling of heat transfer and electric conduction is important to accurately predict the performance of TEs. This paper develops a general, three-dimensional numerical model of TEs with consideration of coupling of temperature field and electric potential field. The model is used to figure out the performance of thermoelectric coolers (TECs) with the temperature-dependent thermal conductivity, electric conductivity, and Seebeck coefficient of semiconductor materials. A miniature TEC is considered and $Bi_2(Te_{0.94}Se_{0.06})_3$ and $(Bi_{0.25}Sb_{0.75})Te_3$ are selected as the n-type and p-type thermoelectric materials, respectively. The effect of parameters such as the temperature difference and the current is investigated under conditions of variable material properties as well as radiation and convection heat transfer occurred between the TEC and the ambient gas. The results show that the variable properties and the heat losses to the ambient gas have significant effects on the cooling capacity and the coefficient of performance (COP) of the TEC. Three-dimensional temperature distributions within the semiconductors is observed under convective boundary condition and it becomes remarkable at large temperature differences and high currents.

1. Introduction

Recently, the research and development of thermoelectric devices (TEs) have attracted a great deal of attention because of their potential applications in green energy and energy management [1–3]. TEs can be classified into two different groups; one is the thermoelectric generator (TEG) which converts heat into electricity [4–15] and the other is the thermoelectric cooler (TEC) which converts electricity into heat [16–43]. Compared to conventional mechanical providers of heating, cooling and electric power generation, such as air conditioners, refrigerators, heat pumps and turbine engines, TEs are more robust, compact and noiseless because they are solid state heat engines that use electrons and holes as working fluid, so that neither moving parts nor real fluids are needed [1,2].

TEs contain over hundred pairs of thermoelectric elements (p–n junctions) connected electrically in series, but thermally in parallel between two planar substrates. The TE performance is closely related to the figure-of-merit of thermoelectric materials, ZT, which is defined as $ZT = \alpha\sigma T/\lambda$, where α is the Seebeck coefficient, σ is the electric conductivity, λ is the thermal conductivity, and T is the absolute temperature at which the properties are measured [2,3]. The materials with large ZT can improve the TE performance significantly [1–3], thus, high electric conductivity, high Seebeck coefficient, and low thermal conductivity are desired for thermoelectric materials. In addition, the TE performance can also be improved by optimization of its geometric design and operating conditions.

So far, a number of models have been proposed to analyze the heat transfer and performance of TEs. The models can be divided into two types. One is the energy equilibrium model or zero-dimensional model [4–8,11,18,21,22,24,25,27,29,31,33,39], where heat balance equations (algebraic equation) at the hot junction and

* Corresponding author. State Key Laboratory of Alternate Electrical Power System with Renewable Energy Sources, North China Electric Power University, Beijing 102206, China. Tel./fax: +86 10 62321277.
E-mail address: wangxd99@gmail.com (X.-D. Wang).

0360-5442/$ – see front matter © 2012 Elsevier Ltd. All rights reserved.
http://dx.doi.org/10.1016/j.energy.2012.09.019

the cold junction are constructed, respectively, without solving energy differential equation. The advantage of these models is that it can obtain the analytical expressions for the TE performance, but their accuracy is limited due to gross simplifying assumptions. For example, Joule heat and Thomson heat are generally assumed to be equally distributed to the hot and cold junctions. The other is the one-dimensional [9,17,19,23,26,28] or three-dimensional [10,30,38,43] heat transfer model, where Fourier's heat conduction equation (differential equation) with Joule heat and/or Thomson heat as inner heat sources is modeled and solved. Then the TE performance can be obtained by solving temperature distributions. In these two types of models, the p–n junction is usually simplified as an individual bulk phase so that the difference in the thermal behavior between p-type and n-type semiconductors is not possible to be distinguished and evaluated [4–11,17–19,21–29,31,33,39]. Recently, some researches treat the p-type and n-type semiconductors as two separate parts and consider the difference in temperature between the two elements [30,38,43]. Furthermore, in these models, the current is assumed to be transported only along the height direction (z direction) of semiconductors with uniform current density over the cross-section (x–y plane) of semiconductors, thus, the current density vector $\vec{J}(x,y,z)$ within the semiconductors can be simplified as a scalar, or, $J_x = J_y = 0, J_z = I/A$, where I is the total current through the TE element, and A is the cross-sectional area of semiconductors. So, the electric potential equation is not needed to be solved.

In fact, there is coupling of temperature field and electric potential field within semiconductors. First, the electric potential through semiconductors includes two parts: the electric potential due to current flowing through the semiconductors and the thermoelectric potential produced by temperature gradient due to Seebeck effect. The Seebeck coefficient and electric conductivity of semiconductor materials are all temperature-dependent, and the Seebeck thermoelectric potential is a function of temperature gradient. As a result of three-dimensional temperature distribution, the electric potential and current density are also three-dimensional. Second, in the energy equation, the source terms of Joule heat and Thomson heat are the functions of current density, which are determined in terms of the electric potential distribution. Thus, a multidimensional, multiphysics model with coupling of temperature field and electric potential field is needed to predict the TE performance more accurately without assumption of uniform current density and to be applied to various thermoelectric materials and comprehensive operation conditions.

Based on the above analysis, this paper firstly focuses on the construction of a general model with coupling of temperature field and electric potential field, which can be used to investigate the performances of both the TEG and the TEC. Then a TEC is selected as an example to measure the ability of the present model. The effects of the temperature-dependent properties of p-type and n-type semiconductors and the convective boundary conditions at the TEC side surfaces on the TEC cooling capacity and coefficient of performance (COP) are analyzed. The results are compared to those with constant property assumption and adiabatic boundary conditions extensively adopted by previous models.

2. Model

A TEC device is formed from a number of thermoelectric elements, connected electrically in series and thermally in parallel. With consideration of periodicity, a TEC element is extracted and is shown in Fig. 1, which is composed of p-type and n-type semiconductor columns with the same square cross-section sandwiched between two metallic interconnectors. The interconnectors and semiconductors have heights of H_1 and H_2, and the side length of the cross-section for semiconductors is L_2 with the distance of L_1 between p-type and n-type semiconductors.

The current carriers are electrons and holes in the p-type and n-type semiconductors, respectively. When a direct current passes from the p-type semiconductor to the n-type semiconductor, holes in the p-type semiconductors and electrons in the n-type semiconductors are all transported from bottom to top along the semiconductor height direction (plus z axis direction), the corresponding Peltier heats will be generated at the interface between interconnectors and semiconductors. The heat is adsorbed on the bottom of semiconductors and is liberated on the top of semiconductors due to Peltier effect, which causes that the bottom is cooled and the top is heated, and forms a cold junction and a hot junction with temperatures of T_L and T_H, respectively. When the temperature difference $\Delta T = T_H - T_L$ is established between the hot and cold junctions, a Seebeck electric potential is generated and the potential is proportional to the temperature difference. The temperature difference also drives the heat to conduct back from the hot junction to the cold junction (Fourier's heat conduction), weakening the cooling capacity of the TEC. The TEC element can be regarded as the combination of a series of infinitesimal Peltier junctions and each of them individually absorbs and liberates heat. Thus, under the action of current and temperature gradient,

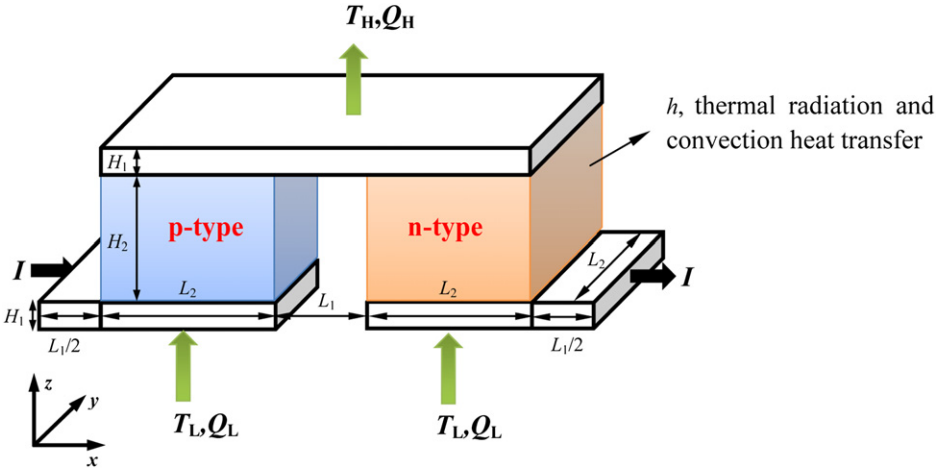

Fig. 1. Schematic diagram of the TEC element.

Thomson heat will be produced within the TEC element. In addition, heat will be generated along the thermoelectric element due to Joule heating, and heat will also be liberated from TEC element to the ambient gas by thermal radiation and convection. Thus, however, cooling capacity cannot be as strong as the Peltier heat pumping rate; it should be determined by the combination of Peltier heat, Fourier's heat conduction, Joule heat, Thomson heat, and heat losses to the ambient gas caused by radiation and convection.

Based on the above analysis, a TEC model with coupling of temperature field and electric potential is constructed in the present paper. It is noted that the model can also be applied to investigate the performance of the TEG, the difference from TEC modeling is that heat should be supplied to hot junction to produce electric potential with the corresponding boundary conditions.

The energy equation for the interconnector, the p-type and n-type semiconductors can be expressed as

$$\nabla\cdot(\lambda_{\mathrm{i}}\nabla T)+\frac{J^2}{\sigma_{\mathrm{i}}}-\beta_{\mathrm{i}}\vec{J}\cdot\nabla T = 0 \tag{1}$$

$$\nabla\cdot(\lambda_{\mathrm{p}}\nabla T)+\frac{J^2}{\sigma_{\mathrm{p}}}-\beta_{\mathrm{p}}\vec{J}\cdot\nabla T = 0 \tag{2}$$

$$\nabla\cdot(\lambda_{\mathrm{n}}\nabla T)+\frac{J^2}{\sigma_{\mathrm{n}}}-\beta_{\mathrm{n}}\vec{J}\cdot\nabla T = 0 \tag{3}$$

where λ_{i}, λ_{p}, and λ_{n} are the thermal conductivities for interconnector, p-type and n-type semiconductors, respectively. The second and third terms on the left side in Eqs. (1)–(3) denote Joule heat and Thomson heat, respectively. $J(x, y, z)$ is the local current density, σ_{i}, σ_{p}, and σ_{n} are the electric conductivities for interconnector, p-type and n-type semiconductors, respectively. β_{i}, β_{p} and β_{n} are the Thomson coefficients for interconnector, p-type and n-type semiconductors which can be expressed as:

$$\beta = T\frac{\mathrm{d}\alpha}{\mathrm{d}T} \tag{4}$$

where α is the Seebeck coefficient. It is noted that constant Seebeck coefficient implies that the Thomson effect is ignored. Theoretically, the Thomson effect cannot be ignored when high temperature gradient occurs within semiconductors. Huang et al. [26] and Chen et al. [43] have confirmed that TEC performance could be improved not only by increasing the figure-of-merit of thermoelectric materials but also by taking the Thomson effect into account. The transport of electrons and holes in semiconductors are driven by electric potential, hence, the electric potential field is needed to be solved as follows:

$$\nabla\cdot(\sigma(\nabla\phi-\alpha\nabla T)) = 0 \tag{5}$$

where ϕ is the electric potential, and $\alpha\nabla T$ is Seebeck electromotive force coming from Seebeck effect. Once ϕ is determined, the electric field can be calculated by the following equation:

$$\vec{E} = -\nabla\phi+\alpha\nabla T \tag{6}$$

Thus, the current density vector in Eqs. (1)–(3) can be calculated as follows:

$$\vec{J} = \sigma\vec{E} \tag{7}$$

Minnich et al. [3] proposed that the properties of some thermoelectric materials are strongly temperature-dependent; hence for the purpose of constructing a general model of TEC, the variable properties should be considered. In the present model, the thermal conductivity, electric conductivity and Seebeck coefficient are all assumed to be the functions of temperature as follows:

$$\lambda(T) = \lambda(T_0)\left[1+A_1(T-T_0)+A_2(T-T_0)^2\right] \tag{8}$$

$$\frac{1}{\sigma(T)} = \rho(T) = \rho(T_0)\left[1+B_1(T-T_0)+B_2(T-T_0)^2\right] \tag{9}$$

$$\alpha(T) = \alpha(T_0)\left[1+C_1(T-T_0)+C_2(T-T_0)^2\right] \tag{10}$$

where T_0 is the reference temperature; $\lambda(T_0)$, $\rho(T_0)$, and $\alpha(T_0)$ are the thermal conductivity, electric resistivity, and Seebeck coefficient at reference temperature of T_0, respectively; A_1, A_2, B_1, B_2, C_1, and C_2 are the fitted parameters determined by experimental data.

The governing equations (1)–(3) and (5)–(7) are solved iteratively to obtain the distributions of temperature and electric potential in the p-type and n-type semiconductors. The boundary conditions adopted are:

$$T_{\mathrm{i}}|_{z=0} = T_{\mathrm{L}} \tag{11}$$

$$T_{\mathrm{i}}|_{z=2H_1+H_2} = T_{\mathrm{H}} \tag{12}$$

The Peltier heat will be generated at the interface between semiconductor and interconnector, thus, the temperature and heat flux are assumed to be continuous for this interface and can be expressed as,

On the interface of $z = H_1$, $L_1/2 < x < L_1/2 + L_2$, $0 < y < L_2$:

$$T_{\mathrm{i}}|_{z=H_1} = T_{\mathrm{p}}|_{z=H_1} \tag{13}$$

$$-\lambda_{\mathrm{i}}\left.\frac{\partial T_{\mathrm{i}}}{\partial z}\right|_{z=H_1}+\alpha_{\mathrm{i}}TJ_z|_{z=H_1} = -\lambda_{\mathrm{p}}\left.\frac{\partial T_{\mathrm{p}}}{\partial z}\right|_{z=H_1}+\alpha_{\mathrm{p}}TJ_z|_{z=H_1} \tag{14}$$

On the interface of $z = H_1$, $3L_1/2 + L_2 < x < 3L_1/2 + 2L_2$, $0 < y < L_2$:

$$T_{\mathrm{i}}|_{z=H_1} = T_{\mathrm{n}}|_{z=H_1} \tag{15}$$

$$-\lambda_{\mathrm{i}}\left.\frac{\partial T_{\mathrm{i}}}{\partial z}\right|_{z=H_1}+\alpha_{\mathrm{i}}TJ_z|_{z=H_1} = -\lambda_{\mathrm{n}}\left.\frac{\partial T_{\mathrm{n}}}{\partial z}\right|_{z=H_1}+\alpha_{\mathrm{n}}TJ_z|_{z=H_1} \tag{16}$$

On the interface of $z = H_1 + H_2$, $L_1/2 < x < L_1/2 + L_2$, $0 < y < L_2$:

$$T_{\mathrm{i}}|_{z=H_1+H_2} = T_{\mathrm{p}}|_{H_1+H_2} \tag{17}$$

$$-\lambda_{\mathrm{p}}\left.\frac{\partial T_{\mathrm{p}}}{\partial z}\right|_{z=H_1+H_2}+\alpha_{\mathrm{p}}TJ_z|_{z=H_1+H_2} = -\lambda_{\mathrm{i}}\left.\frac{\partial T_{\mathrm{i}}}{\partial z}\right|_{z=H_1+H_2}+\alpha_{\mathrm{i}}TJ_z|_{z=H_1+H_2} \tag{18}$$

On the interface of $z = H_1 + H_2$, $3L_1/2 + L_2 < x < 3L_1/2 + 2L_2$, $0 < y < L_2$:

$$T_{\mathrm{i}}|_{z=H_1+H_2} = T_{\mathrm{n}}|_{z=H_1+H_2} \tag{19}$$

$$-\lambda_{\mathrm{n}}\left.\frac{\partial T_{\mathrm{n}}}{\partial z}\right|_{z=H_1+H_2}+\alpha_{\mathrm{n}}TJ_z|_{z=H_1+H_2} = -\lambda_{\mathrm{i}}\left.\frac{\partial T_{\mathrm{i}}}{\partial z}\right|_{z=H_1+H_2}+\alpha_{\mathrm{i}}TJ_z|_{z=H_1+H_2} \tag{20}$$

Völklein et al. [17] and Yao [44] proposed that the thermal radiation and convection heat transfer between the

semiconductors and the ambient gas cannot be negligible for microcooler. Therefore, the convective boundary conditions are assumed on the side surfaces of p-type and n-type semiconductors and interconnector in the present model, or:

$$-\lambda\frac{\partial T}{\partial n} = h(T - T_\infty) \tag{21}$$

where, h is the total heat transfer coefficient including the contribution of natural convective heat transfer and radiation heat transfer, and $h = 0$ W m^{-2} K^{-1} denotes adiabatic boundary conditions adopted in the majority of previous models. T_∞ is the ambient temperature assumed to be 293 K here.

The electric boundary conditions for TEC element are assumed to be that the inlet current is constant and outlet electric potential is zero, or:

$$I|_{x=0} = \text{constant} \quad 0 < y < L_2, \ \ 0 < z < H_1 \tag{22}$$

$$\phi|_{x=2L_1+2L_2} = 0 \quad 0 < y < L_2, \ \ 0 < z < H_1 \tag{23}$$

On the other surfaces, the current cannot flow out of TEC element, thus, we have:

$$\vec{J} \cdot \vec{n} = 0 \tag{24}$$

There are two parameters used to evaluate the performance of TEC, cooling capacity Q_L and coefficient of performance (COP). Q_L is defined as the heat absorbed from the cold junction, and COP is defined as the ratio of cooling capacity to electric power expressed as:

$$\text{COP} = \frac{Q_L}{P} = \frac{Q_L}{IV} \tag{25}$$

where P is the electric power, V is the electric potential difference through the TEC element. When side surfaces of TEC element are adiabatic, based on the energy conservation, we have:

$$P = Q_H - Q_L \tag{26}$$

where Q_H is the heat dissipated rate from hot junction. Thus, with adiabatic boundary conditions, the COP is also calculated by the following equation, or:

$$\text{COP} = \frac{Q_L}{Q_H - Q_L} \tag{27}$$

It is noted that the COP was calculated only by Eq. (27) in the previous models because the electric potential difference is unknown.

3. Model validation

The n-type and p-type semiconductors are assumed to be $Bi_2(Te_{0.94}Se_{0.06})_3$ and $(Bi_{0.25}Sb_{0.75})Te_3$ with temperature-dependent properties, respectively. The copper is selected as interconnector with constant properties due to weak thermoelectric effect. Table 1 lists all the parameters in Eqs. (8)–(10) for the n-type and p-type semiconductors and the copper interconnector.

3.1. Grid independence examination

In order to guarantee that the simulation results are independent on the grid, four different grid schemes were tested. The geometric parameters of the TEC element and corresponding grid number for test are listed in Table 2. The temperature difference between the hot and cold junctions is assumed to be $\Delta T = T_H - T_L = 0$ K with the total heat transfer coefficient $h = 0$ W m^{-2} K^{-1}. Fig. 2 shows the cooling capacity Q_L and COP of the TEC element as functions of the current I for four grid schemes. At $I < 1.6$ A, four grid schemes have almost the same Q_L and COP, while at $I > 1.6$ A, the differences for Q_L and COP predicted by four grid schemes occur. The maximum deviation between Grid (ii) and Grid (iii) is 2.18%, it reduces to 0.62% for Grid (iii) and Grid (iv). Hence, to save computation efforts without loss in accuracy, the Grid (iii) is adopted.

3.2. Validation of model self-consistency

The temperature filed and electric potential field are coupled in the present model, the electric potential difference V through the TEC element can be solved directly as shown in Fig. 3. Thus, the electric power P can be calculated as $P_1 = I \times V$. With the assumption of adiabatic boundary condition on the side surfaces of TEC element, the electric power can also be calculated by $P_2 = Q_H - Q_L$ due to energy balance. The electric powers calculated by two approaches are compared and shown in Fig. 3. The maximum relative deviation $(P_2 - P_1)/P_1$ for various currents is only −0.09%, indicating that the present model has complete self-consistency.

3.3. Comparison between numerical model and theoretical solution

In order to verify the present model, the temperature distributions predicted by the present model and by one-dimensional theoretical solution [26] are compared. In the theoretical solution, the properties of semiconductors, including the thermal conductivity, electric conductivity, and Seebeck coefficient, are all assumed to be constant with adiabatic boundary conditions on the side surfaces of TEC element. It is noted again that constant Seebeck coefficient implies ignored Thomson effect, which is applicable for small temperature gradient within the semiconductors. With these conditions, one-dimensional theoretical solution for energy equation can be expressed [26]:

$$\frac{T(z) - T_L}{T_H - T_L} = \frac{1}{2}\frac{I^2H_2^2}{\lambda\sigma A^2(T_H - T_L)}\left(\frac{z}{H} - \frac{z^2}{H^2}\right) + \frac{z}{H} \tag{28}$$

The comparison of temperature distributions between the present model and Eq. (28) is shown in Fig. 4, in which the geometric parameters of TEC element are the same as Section 3.1

Table 1
Parameters in Eqs. (8)–(10) for thermoelectric materials ($T_0 = 300$ K).

Material	Thermal conductivity			Electric resistivity			Seebeck coefficient		
	λ_0 (W m^{-1} K^{-1})	A_1 (K^{-1})	A_2 (K^{-2})	ρ_0 (Ω m)	B_1 (K^{-1})	B_2 (K^{-2})	α_0 (V K^{-1})	C_1 (K^{-1})	C_2 (K^{-2})
p-type	1.472	-1.29×10^{-3}	1.35×10^{-5}	8.826×10^{-6}	5.88×10^{-3}	8.93×10^{-6}	2.207×10^{-4}	1.55×10^{-3}	-3.15×10^{-6}
n-type	1.643	-9.80×10^{-4}	1.56×10^{-5}	8.239×10^{-6}	4.70×10^{-3}	2.67×10^{-6}	-2.23×10^{-4}	5.62×10^{-4}	-4.65×10^{-6}
Interconnector	400	0	0	1.7×10^{-9}	0	0	6.5×10^{-6}	0	0

Table 2
The geometric parameters and test grid numbers for TEC.

		L_1	L_2	L_3	H_1	H_2
Geometry	Value	0.1 mm	0.5 mm	0.2 mm	0.1 mm	1.0 mm
Grid i	Grid number	2	10	4	2	20
Grid ii	Grid number	4	20	8	4	40
Grid iii	Grid number	5	25	10	5	50
Grid iv	Grid number	6	30	12	6	60

with $T_L = 300$ K, $T_H = 330$ K, $h = 0$ W m^{-2} K^{-1}, and $I = 1.7$ A. The temperature distributions for four different property conditions are simulated by the present model: 1) all properties are constant and exactly the same as the theoretical solution; 2) temperature-dependent α with constant λ and σ; 3) constant α with temperature-dependent λ and σ; 4) all properties are temperature-dependent.

Fig. 4 shows that the maximum temperature occurs inside semiconductors for all four cases due to thermoelectric effect. The temperature of p-type semiconductor is larger than that of n-type semiconductor because λ_p of p-type semiconductor is 1.472 W m^{-1} K^{-1} at $T = 300$ K, which is lower than $\lambda_n = 1.643$ W m^{-1} K^{-1} for n-type semiconductor. It can be seen that the temperature distribution curves of p-type and n-type semiconductors predicted by the present model with the constant properties and adiabatic boundary conditions coincide perfectly with the theoretical solution, validating the model. However, for the other three cases with variable properties, the temperatures are higher than that with constant properties and maximum temperature difference reaches to 13.25 K. The comparison demonstrates that the temperature-dependent properties should be taken into account to predict the TEC performance accurately. Fig. 4 also confirms the results reported by previous investigations [26,43], the Thomson effect could influence significantly on the TEC performance, which decreases the temperature of semiconductors, especially for the p-type semiconductor with lower thermal conductivity.

4. Results and discussion

The cooling capacity Q_L and COP of TEC are closely related to its operating conditions, including the current and the temperature difference between the hot and cold junctions. The effect of these parameters on the TEC performance has been discussed extensively in the previous investigations, however, the models do not couple

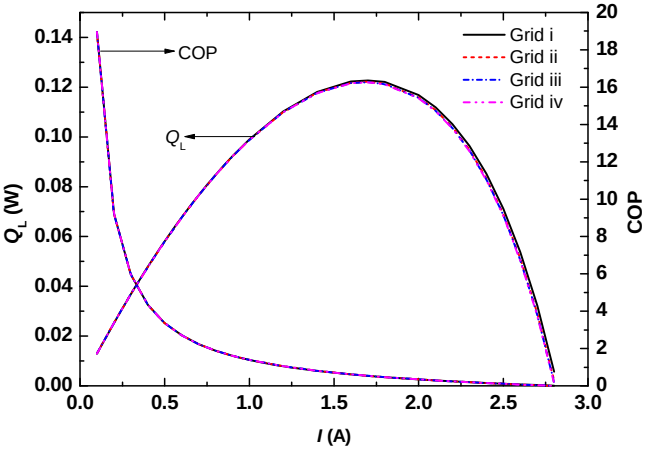

Fig. 2. Grid independence examinations.

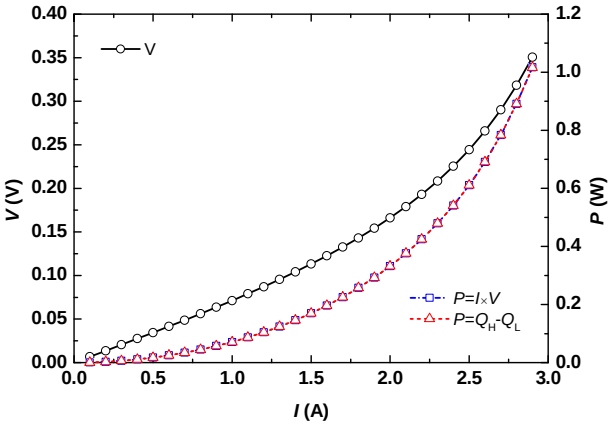

Fig. 3. Electric potential differences and electric powers at various currents for the TEC element.

the temperature field and the electric potential field and generally assumed constant properties of semiconductors and adiabatic boundary conditions on the side surfaces of TEC, and hence the results are applicable only at specific conditions. This work will analyze the effect of the properties (Section 4.1) and convective boundary conditions (Section 4.2) on the performance of the TEC

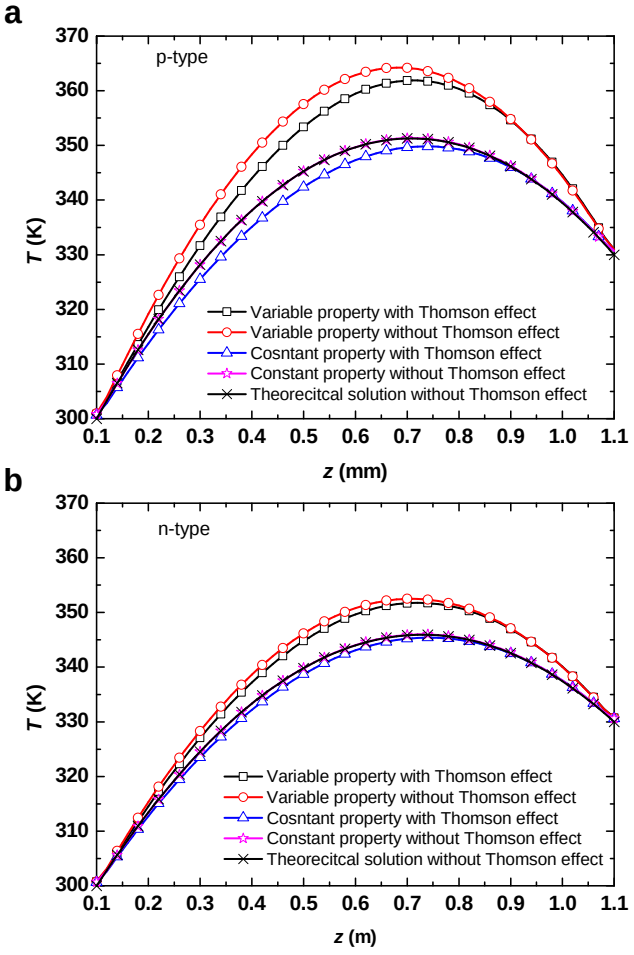

Fig. 4. Comparison of temperature distributions predicted by the present model and calculated by the one-dimensional theoretical solution: (a) p-type semiconductor; (b) n-type semiconductor.

element in a wide range of the current and temperature difference between the hot and cold junctions using the coupled model described in Section 2.

4.1. Effect of semiconductor properties

The three-dimensional analysis is carried out with TEC element listed in Table 2. The temperature of cold junction is fixed to $T_L = 300$ K and the temperature difference between the hot and cold junctions is assumed to be $\Delta T = 0$ K, 20 K, 40 K, 60 K, 80 K, and 100 K, respectively. The adiabatic boundary condition, $h = 0$ W m^{-2} K^{-1}, is adopted in this section to highlight the effect of semiconductor properties.

Fig. 5 illustrates the cooling capacities of the TEC element as a function of current with various ΔT under constant and variable property models, respectively. For the constant property model, Q_L firstly increases and then drops as the current further increases, hence there exists maximum cooling capacity $Q_{L,max}$. At $\Delta T = 0$ K, effective working currents, defined as the current when $Q_L \geq 0$ W, are 0 A $< I <$ 3.940 A, and the current corresponding to $Q_{L,max}$ is $(3.940 - 0)/2 = 1.970$ A, implying that the Q_L–I curve is completely symmetric. As ΔT is increased, the effective working current interval is reduced but the Q_L–I curve remains symmetric with the same current of 1.970 A corresponding to $Q_{L,max}$. The maximum cooling capacity $Q_{L,max}$ is reduced as ΔT is increased due to elevated Fourier's heat conduction. The constant decrease rate ($dQ_{L,max}/dT$) of 7.75×10^{-4} W/K is observed, and similar results were also reported by Lee and Kim [30]. For example, at $\Delta T = 0$ K, $Q_{L,max} = 0.1302$ W; at $\Delta T = 20$ K, $Q_{L,max} = 0.1302 - 7.75 \times 10^{-4} \times 20 = 0.1147$ W; at $\Delta T = 100$ K, $Q_{L,max} = 0.1302 - 7.75 \times 10^{-4} \times 100 = 0.0527$ W.

Fig. 5 indicates that the Q_L–I curves for variable property model are distinct from those for constant property model. First, the maximum effective working current is decreased significantly, the Q_L–I curves no longer have symmetry. At low currents, the Joule heat and Thomson heat produced within the semiconductors are so small that the temperature distributions predicted by the constant and variable property models are nearly identical (Fig. 6), leading to a small difference in cooling capacity Q_L between the two models. As the current is raised, the temperature distributions predicted by the two models become remarkably different because the Joule heat and Thomson heat are increased rapidly, and the variable property model predicts a higher temperature distribution. Higher temperature distribution results in a stronger Fourier's heat conduction from hot junction to cold junction, thus, the cooling capacity Q_L and the corresponding maximum effective working current are decreased. Second, maximum cooling capacity $Q_{L,max}$ is reduced significantly for the variable property model, and the currents corresponding to $Q_{L,max}$ at different ΔT are no longer the

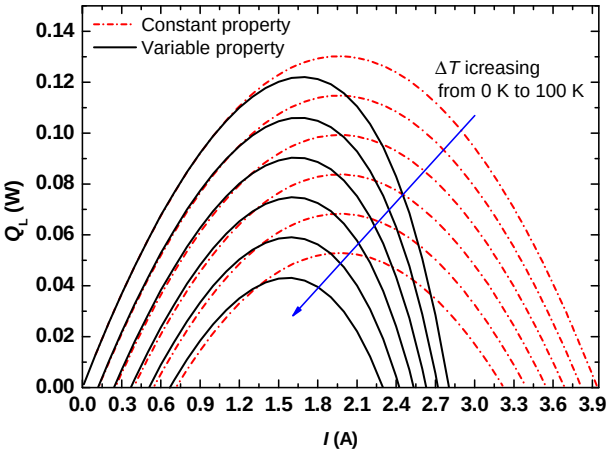

Fig. 5. Cooling capacity of the TEC element for constant and variable properties at various temperature differences.

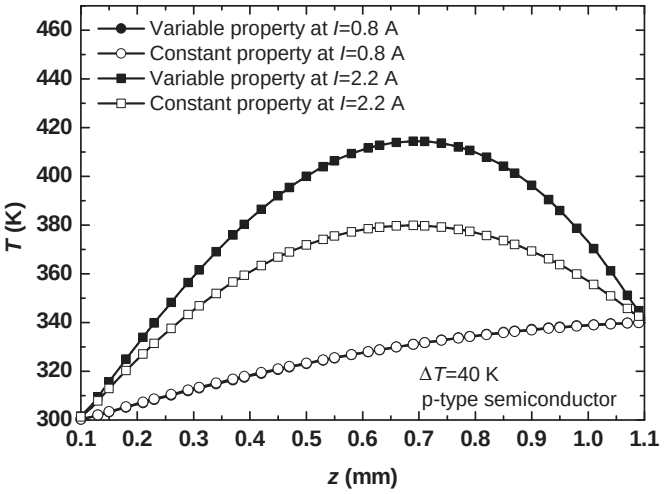

Fig. 6. Temperature distributions for p-type semiconductor at different currents for constant and variable properties.

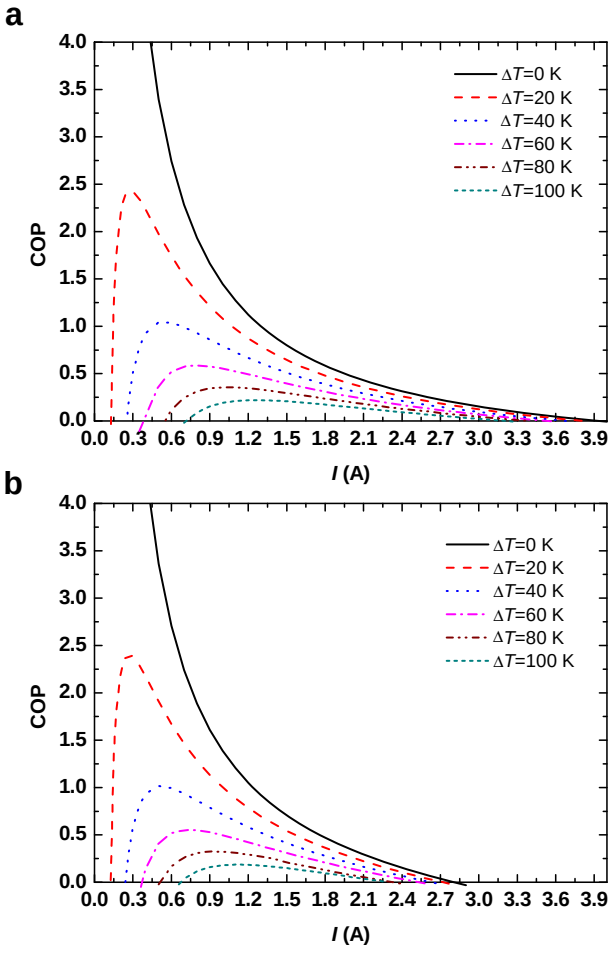

Fig. 7. COP of the TEC element for constant and variable properties at various temperature differences: (a) constant properties; (b) variable properties.

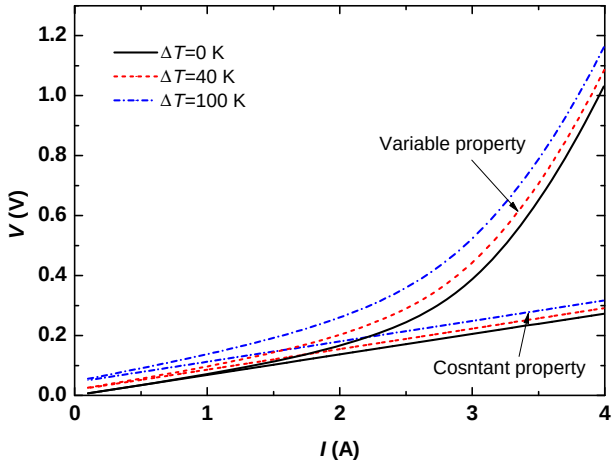

Fig. 8. *I–V* curves of the TEC element for constant and variable properties.

same but decrease as ΔT increased. For example, at $\Delta T = 0$ K, $Q_{L,max} = 0.1220$ W, the corresponding current is 1.685 A; at $\Delta T = 100$ K, $Q_{L,max} = 0.0431$ W, the corresponding current decreases to 1.575 A. Furthermore, similar as the constant property model, $Q_{L,max}$ is decreased as ΔT increased and the decrease rate still remains constant value of 7.89×10^{-4} W/K slightly lower than 7.75×10^{-4} W/K for the constant property model.

Fig. 7 shows the COPs of TEC element as functions of current and temperature difference for the two models. At $\Delta T = 0$ K, the COP is reduced monotonously as the current increased for both models, and there is no maximum COP. However, at $\Delta T > 0$ K, the COP reaches its peak value COP_{max} at a certain current and then monotonically drops as the current increases further. It is also noted that the COP decreases as ΔT increased. The *I–V* curves of TEC element for the two models are shown in Fig. 8. It is seen that the electric potential difference through the TEC element increases as ΔT increased for two models. Thus, higher ΔT not only decreases the cooling capacity but also increases the electric potential difference leading to the reduced COP. Fig. 8 also shows that the electric potential difference increased almost linearly with the current for constant property model, which is lower than that for variable property model, the discrepancy between two models becomes more significant at high currents and large ΔT. The discrepancy of the electric potential differences comes from the difference of temperature distributions predicted by two models. The Seebeck electric potential gradient is equal to the product of Seebeck coefficient and the temperature gradient. The higher temperature gradient and positive temperature effect of Seebeck coefficient cause a larger Seebeck potential through the TEC element for the variable property model. It is noted from Fig. 7 that the current corresponding to COP_{max} is elevated as ΔT increased, and this current is different from the current corresponding to $Q_{L,max}$, which means that the requirement of maximum cooling capacity and COP cannot be met simultaneously.

It can be seen from Fig. 7 that for $\Delta T = 20$ K, $COP_{max} = 2.403$ at current of 0.270 A for the variable property model, and $COP_{max} = 2.434$ at current of 0.281 A for the constant property model with relative deviation of $(2.434 - 2.403)/2.403 = 1.3\%$. However, at $\Delta T = 100$ K, $COP_{max} = 0.187$ at current of 1.116 A for the variable property model, and $COP_{max} = 0.220$ at current of 1.262 A for the constant property model with relative deviation of $(0.220 - 0.187)/0.187 = 17.6\%$. Therefore, the constant property model overestimates the COP_{max} and the degree of the overestimation increases with ΔT increased. This can be explained by the following two reasons. First, as ΔT increases, the constant property model overestimates the cooling capacity (Fig. 5) and underestimates the electric potential difference (Fig. 8) more significantly. Second, the current corresponding to COP_{max} increases at larger ΔT, higher current further increases the degree of overestimation of the constant property model. The above results indicate that the temperature-dependent properties of semiconductors are necessary to take into account for TEC modeling at large ΔT and higher *I*.

4.2. Effect of convective boundary condition

During TEC operation, the temperature of TEC is generally higher than the ambient temperature; hence, the heat will be transferred from the TEC to the ambient gas by radiation and convection. In the previous models, the adiabatic boundary conditions were adopted extensively, only a few models considered the effect of radiation and convection heat transfer on the TEC performance [17,26,38]. In these models, the radiation heat transfer h_r was linearized under the assumption of small temperature difference $((T_{p,n} - T_\infty)/T_\infty << 1)$ and a total heat transfer coefficient combining the radiation heat transfer coefficient h_r and the convection heat transfer coefficient h_c, which can be expressed as $h = h_c + h_r = h_c + 4\varepsilon\sigma_B T_\infty$, is used to estimate the heat transfer between the TEC and the ambient. However, different values of *h* were assumed in these models, for example, *h* is assumed to be100 W m^{-2} K^{-1} in Ref. [17], 50 W m^{-2} K^{-1} in Ref. [26], and 5–15 W m^{-2} K^{-1} in Ref. [38]. In the present model, the value of *h* is assumed to be varied from 0 to 200 W m^{-2} K^{-1}, it is noted that a little higher *h* (=200 W m^{-2} K^{-1}) is employed here to highlight the effect of convective boundary condition.

The calculations are carried out with the geometry of TEC element identical to that in Section 4.1. The temperature of the cold junction is set at 300 K, and the temperature of the hold junction is 300 K, 340 K, and 400 K, respectively. Thus, the temperature difference is 0 K, 40 K, and 100 K, respectively. In addition, the temperature-dependent properties are adopted.

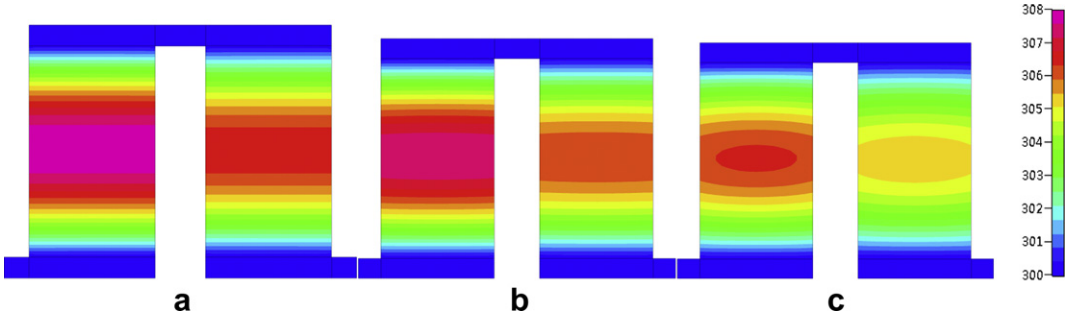

Fig. 9. Effect of the total heat transfer coefficient on the temperature distributions on the middle cross-section ($y = 0.25$ mm) at $\Delta T = 0$ K and $I = 0.8$ A: (a) $h = 0$ W m^{-2} K^{-1}; (b) $h = 50$ W m^{-2} K^{-1}; (c) $h = 200$ W m^{-2} K^{-1}.

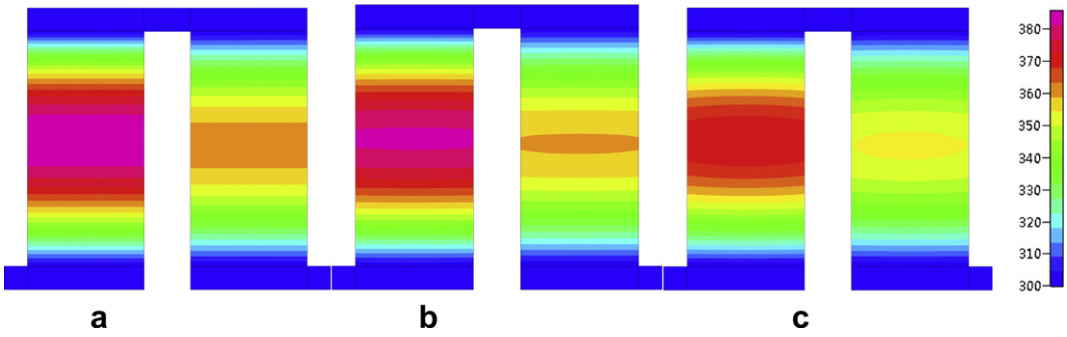

Fig. 10. Effect of the total heat transfer coefficient on the temperature distributions on the middle cross-section ($y = 0.25$ mm) at $\Delta T = 0$ K and $I = 2.2$ A: (a) $h = 0$ W m^{-2} K^{-1}; (b) $h = 50$ W m^{-2} K^{-1}; (c) $h = 200$ W m^{-2} K^{-1}.

Figs. 9 and 10 show the effect of the total heat transfer coefficient on the temperature distributions on the middle cross-section ($y = 0.25$ mm) at $\Delta T = 0$ K with $I = 0.8$ A and 2.2 A, respectively. It is seen again that the p-type semiconductor has higher temperature than the n-type semiconductor due to its lower thermal conductivity and higher electric resistivity. At low current of $I = 0.8$ A, there is a small amount of Joule heat and Thomson heat produced inside semiconductors, the difference of temperature distributions for various total heat transfer coefficients is small. As the total heat transfer coefficient increases, the temperatures of the semiconductors are reduced slightly since the heat loss to the ambient is enhanced. With $h = 0$ W m^{-2} K^{-1}, the maximum temperature for the p-type semiconductor is $T_{p,max} = 308.0$ K and for the n-type semiconductor is $T_{n,max} = 306.6$ K; with $h = 50$ W m^{-2} K^{-1}, $T_{p,max} = 307.6$ K, and $T_{n,max} = 306.3$ K; with $h = 200$ W m^{-2} K^{-1}, $T_{p,max} = 306.4$ K, $T_{n,max} = 305.3$ K. At high current of $I = 2.2$ A, however, the Joule heat and Thomson heat produced inside the semiconductors increase significantly, causing that the temperatures of both the p-type and n-type semiconductors are far larger than those at $I = 0.8$ A. Increased temperature difference between the semiconductors and the ambient enhances the heat loss to the ambient and hence increases the effect of total heat transfer coefficient. The above analysis can be proved by the fact that with $h = 0$ W m^{-2} K^{-1}, $T_{p,max} = 385.8$ K, and $T_{n,max} = 361.2$ K; with $h = 50$ W m^{-2} K^{-1}, $T_{p,max} = 382.3$ K, and $T_{n,max} = 359.2$ K; $h = 200$ W m^{-2} K^{-1}, $T_{p,max} = 373.1$ K, and $T_{n,max} = 354.0$ K. In addition, it is observed that at high total heat transfer coefficient of $h = 200$ W m^{-2} K^{-1}, the isothermal lines near the middle of semiconductors are not parallel to the x-direction, indicating a three-dimensional temperature distribution occurs.

Fig. 11 shows the I–V curves of the TEC element for various h at $\Delta T = 0$ K. At $I < 1.5$ A, h has a very small effect on the I–V curves, while at $I > 1.5$ A, the effect of h is elevated gradually as the current increases. Higher h leads to a reduced electric potential difference through the TEC element and hence a reduced electric power.

The cooling capacity Q_L and the corresponding COP for various h at $\Delta T = 0$ K are shown in Fig. 12. Similar as the electric potential, the effect of h on Q_L is enhanced with the current increased. Increase in h leads to higher Q_L because the heat loss to the ambient decreases the Fourier's heat conduction to cold junction. Fig. 12 also indicates that as h is raised, the effective working current interval increases and the current corresponding to $Q_{L,max}$ moves towards to higher current direction. At $h = 0$ W m^{-2} K^{-1}, the interval is varied from 0 A to 2.806 A with $Q_{L,max} = 0.1220$ W at the current of 1.685 A; at $h = 50$ W m^{-2} K^{-1}, the interval is 0–2.858 A with $Q_{L,max} = 0.1256$ W at the current of 1.722 A; at $h = 200$ W m^{-2} K^{-1}, the interval is 0–3.014 A with $Q_{L,max} = 0.1355$ W at the current of 1823 A. Fig. 12 demonstrates that the COP increases with h increased due to that higher h not only increases Q_L but also decreases V.

The effect of h on the TEC performance is closely dependent on ΔT. Figs. 13 and 14 show the Q_L and the corresponding COP for various h at $\Delta T = 40$ K and $\Delta T = 100$ K, respectively. Similar as $\Delta T = 0$ K, Q_L and COP both increase as h increases and the effect of h becomes more significant at higher currents. The above analyses indicate that the radiation and convection heat transfer between the TEC and the ambient gas are beneficial to improve the TEC performance. It can be expected that the effect of the radiation and

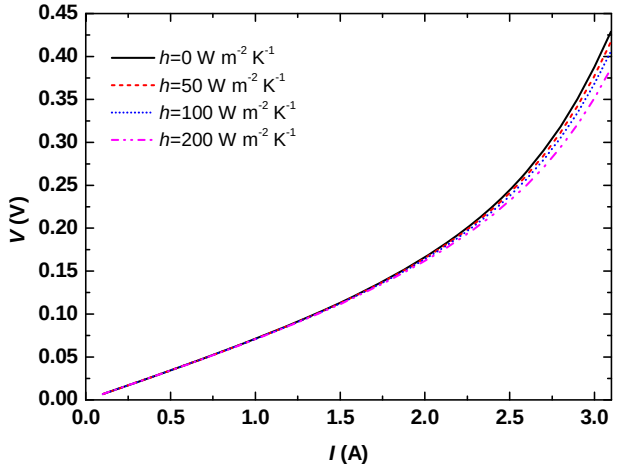

Fig. 11. I–V curves of the TEC element with various convective heat coefficients at $\Delta T = 0$ K.

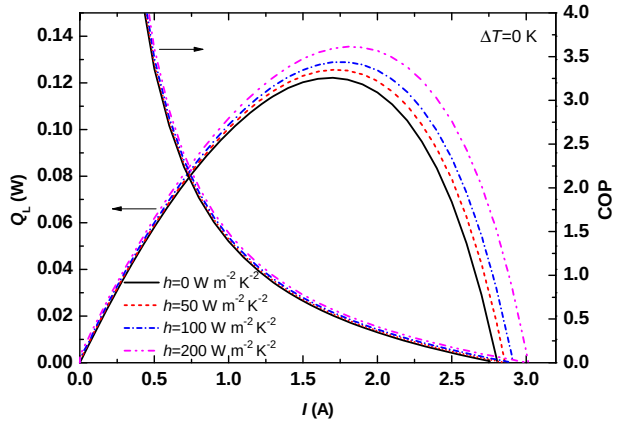

Fig. 12. Performance of the TEL element with various convective heat coefficients at $\Delta T = 0$ K.

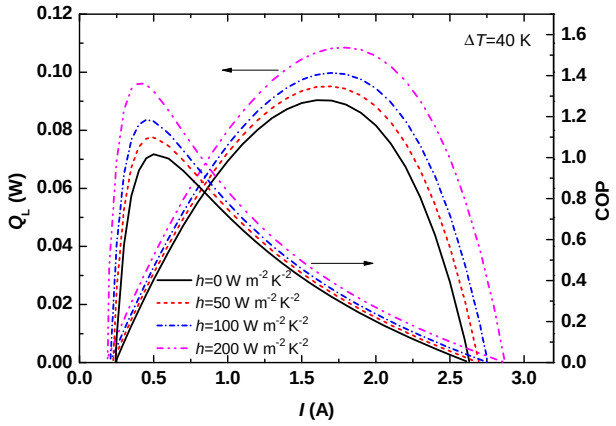

Fig. 13. Performance of the TEC element with various convective heat coefficients at $\Delta T = 40$ K.

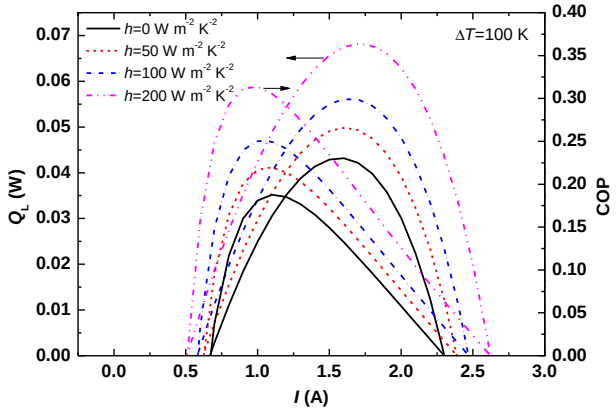

Fig. 14. Performance of the TEC element with various convective heat coefficients at $\Delta T = 100$ K.

convection heat transfer for the TEG is opposite to the TEC, because the heat loss to the ambient gas reduces the temperature difference between the hot and cold junctions and hence reduces the Seebeck electric potential. The comparison of Figs. 12–14 indicates that the effect of h on the TEC performance is elevated as ΔT increases. The reason can be explained as follows. As mentioned before, at high ΔT, there is a stronger Fourier's heat conduction, which causes the heat transferred back from the hot junction to the cold junction and hence leads to a decreased Q_L. With the same h, more heat is absorbed by the ambient gas at higher ΔT due to lager temperature difference between the TEC and the ambient gas, so the effect of Fourier's heat conduction is reduced and Q_L is increased more significantly. Figs. 13 and 14 again confirm that increase in h increases the effective working current interval and causes a move of the current corresponding to $Q_{L,max}$ towards higher current. Oppositely, increase in h causes that the current corresponding COP_{max} moves towards lower current.

5. Conclusions

This paper develops a general, three-dimensional TE model with coupling of the temperature field and the electric potential field. All effect occurred in the TE are taken into account, such as the Joule heating, the Thomson effect, Fourier's heat conduction, the Peltier effect, the radiation and convection heat transfer, and temperature-dependent properties of semiconductor materials. A miniature TEC element with the ratio of cross-sectional area to the height of 0.25 mm is investigated and $Bi_2(Te_{0.94}Se_{0.06})_3$ and $(Bi_{0.25}Sb_{0.75})Te_3$ are selected as the n-type and p-type thermoelectric materials, respectively.

The temperature filed and electric potential field are calculated coupled in the present model, so the electric potential difference through the TEC element can be solved directly. The self-consistency of the model was verified by the fact that the electric powers calculated by two approaches are identical under adiabatic boundary conditions. With constant properties and adiabatic boundary conditions, the temperature distributions within the p-type and n-type semiconductors predicted by the present model agree well with the one-dimensional theoretical solution.

The effects of the properties and convective boundary conditions on the TEC performance are discussed in a wide current and temperature difference range using the present model. The predicted results show that the constant property model overestimates the cooling capacity, the COP, and the effective working current interval of the TEC and underestimates the electric potential compared to the variable property model. Besides, a significantly increased deviation is observed at high currents. The convective boundary conditions cause a three-dimensional temperature distribution within semiconductors. The effect of the radiation and convection heat transfer on the TEC performance increases significantly at high temperature difference between the hot and cold junctions or at high current.

Acknowledgment

This study was supported by the National Natural Science Foundation of China (No. 51276060), by National Basic Research Program of China (No. 2009CB219803), by Program for New Century Excellent Talents in University (No. NCET-11-0635), and by the Fundamental Research Funds for the Central Universities (No. 11ZG01).

References

[1] Riffat SB, Ma X. Thermoelectrics: a review of present and potential applications. Applied Thermal Engineering 2003;23:913–35.
[2] Rowe DM, editor. Thermoelectrics handbook: macro to nano. BocaRaton: CRC Press; 2006.
[3] Minnich AJ, Dresselhaus MS, Ren ZF, Chen G. Bulk nanostructured thermoelectric materials: current research and future prospects. Energy & Environmental Science 2009;2:466–79.
[4] Omer SA, Infield DG. Design optimization of thermoelectric devices for solar power generation. Solar Energy Materials and Solar Cells 1998;53:67–82.
[5] Chen L, Li J, Sun F, Wu C. Performance optimization of a two-stage semiconductor thermoelectric-generator. Applied Energy 2005;82:300–12.
[6] Rodriguez A, Vian JG, Astrain D, Martinez A. Study of thermoelectric systems applied to electric power generation. Energy Conversion and Management 2009;50:1236–43.
[7] Hsiao YY, Chang WC, Chen SL. A mathematic model of thermoelectric module with applications on waste heat recovery from automobile engine. Energy 2010;35:1447–54.
[8] Gou X, Xiao H, Yang S. Modeling, experimental study and optimization on low-temperature waste heat thermoelectric generator system. Applied Energy 2010;87:3131–6.
[9] Montecucco A, Buckle JR, Knox AR. Solution to 1-D unsteady heat conduction equation with internal Joule heat generation for thermoelectric devices. Applied Thermal Engineering 2012;35:177–84.
[10] Chen M, Rosendahl LA, Condra T. A three-dimensional numerical model of thermoelectric generator in fluid power systems. International Journal of Heat and Mass Transfer 2011;54:345–55.
[11] Meng F, Chen L, Sun F. A numerical model and comparative investigation of a thermoelectric generator with multi-irreversibilities. Energy 2011;36:3513–22.
[12] Rezania A, Rosendahl LA. Thermal effect of a thermoelectric generator on parallel microchannel heat sink. Energy 2012;37:220–7.
[13] Wang CC, Hung CI, Chen WH. Design of heat sink for improving the performance of thermoelectric generator using two-stage optimization. Energy 2012;39:236–45.

[14] Chen WH, Liao CY, Hung CI, Huang WL. Experimental study on thermoelectric modules for power generation at various operating conditions. Energy 2012; 45:874–81.
[15] Astrain D, Vian JG, Martinez A, Rodriguez A. Study of the influence of heat exchangers' thermal resistances on a thermoelectric generation system. Energy 2010;35:602–10.
[16] Chen L, Wu C, Sun F. Heat transfer effect on the specific cooling load of refrigerator. Applied Thermal Engineering 1996;16:989–97.
[17] Völklein F, Min G, Rove DM. Modeling of microelectromechanical thermoelectric cooler. Sensors and Actuators 1999;75:95–101.
[18] Huang BJ, Chin CJ, Duang CL. A design method of thermoelectric cooler. International Journal of Refrigeration 2000;23:208–18.
[19] Huang BJ, Duang CL. System dynamic model and temperature control of a thermoelectric cooler. International Journal of Refrigeration 2000;23:197–207.
[20] Chen L, Gong J, Shen L, Sun F, Wu C. Theoretical analysis and experimental confirmation for the performance of thermoelectric refrigerator. Journal of Non-Equilibrium Thermodynamics 2001;26:85–92.
[21] Luo J, Chen L, Sun F, Wu C. Optimum allocation of heat transfer surface area for cooling load and COP optimization of a thermoelectric refrigerator. Energy Conversion and Management 2003;44:3197–206.
[22] Khire RA, Messac A, Dessel SV. Design of thermoelectric pump unit for active building envelope systems. International Journal of Heat and Mass Transfer 2005;48:4028–40.
[23] Xuan XC, Ng KC, Yap C, Chua HT. A general model for studying effects of interface layers on thermoelectric devices performance. International Journal of Heat and Mass Transfer 2002;45:5159–70.
[24] Chein R, Huang G. Thermoelectric cooler application in electronic cooling. Applied Thermal Engineering 2004;24:2207–17.
[25] Cheng YH, Lin WK. Geometric optimization of thermoelectric coolers in a confined volume using genetic algorithms. Applied Thermal Engineering 2005;25:2983–97.
[26] Huang MJ, Yen RH, Wang AB. The influence of the Thomson effect on the performance of a thermoelectric cooler. International Journal of Heat and Mass Transfer 2005;48:413–8.
[27] Cheng YH, Shih C. Maximizing the cooling capacity and COP of two-stage thermoelectric coolers through genetic algorithm. Applied Thermal Engineering 2006;26:937–47.
[28] Chakraborty A, Saha BB, Koyama S, Ng KC. Thermodynamic modeling of a solid state thermoelectric cooling device: temperature-entropy analysis. International Journal of Heat and Mass Transfer 2006;49:3547–54.
[29] Pan Y, Lin B, Chen J. Performance analysis and parametric optimal design of an irreversible multi-couple thermoelectric refrigerator under various operating conditions. Applied Energy 2007;84:882–92.
[30] Lee KH, Kim OJ. Analysis on the cooling performance of the thermoelectric micro-cooler. International Journal of Heat and Mass Transfer 2007;50: 1982–92.
[31] Taylor RA, Solbrekken GL. Comprehensive system-level optimization of thermoelectric devices for electronic cooling applications. IEEE Transaction on Components and Packaging Technologies 2008;31:23–31.
[32] Meng F, Chen L, Sun F. Performance optimization for two-stage thermoelectric refrigerator system driven by two-stage thermoelectric generator. Cryogenics 2009;49:57–65.
[33] Yu J, Wang B. Enhancing the maximum coefficient of performance of thermoelectric cooling modules suing internally cascaded thermoelectric couples. International Journal of Refrigeration 2009;32:32–9.
[34] Meng F, Chen L, Sun F. Extreme working temperature differences for thermoelectric refrigerating and heat pumping devices driven by thermoelectric generator. Journal of Energy Institute 2010;83:108–13.
[35] Meng F, Chen L, Sun F. Multivariable optimization of a two-stage thermoelectric refrigerator driven by a two-stage thermoelectric generator with external heat transfer. Indian Journal of Pure and Applied Physics 2010;48: 731–42.
[36] Meng F, Chen L, Sun F. Performance analysis for two-stage TEC system driven by two-stage TEG obeying Newton's heat transfer law. Mathematical and Computer Modelling 2010;52:586–95.
[37] Meng F, Chen L, Sun F. Multiobjective analyses of physical dimension on the performance of a TEG-TEC system. International Journal of Low-Carbon Technologies 2010;5:193–200.
[38] Cheng CH, Huang SY, Cheng TC. A three-dimensional theoretical model for predicting transient thermal behavior of thermoelectric coolers. International Journal of Heat and Mass Transfer 2010;53:2001–11.
[39] Martinez A, Rodriguez A. Experimental and analytical study on thermoelectric self cooling of devices. Energy 2011;36:5250–60.
[40] Martinez A, Astrain Rodriguez D. Experimental and analytical study on thermoelectric self cooling of devices. Energy 2011;36:5250–60.
[41] Meng F, Chen L, Sun F. Performance prediction and irreversibility analysis of a thermoelectric refrigerator with finned heat exchangers. Acta Physica Polonica A 2011;120:397–406.
[42] Chen L, Meng F, Sun F. Effect of heat transfer on the performance of thermoelectric generator-driven thermoelectric refrigerator system. Cryogenics 2012;52:58–65.
[43] Chen WH, Liao CY, Huang CI. A numerical study on the performance of miniature thermoelectric cooler affected by Thomson effect. Applied Energy 2012;89:464–73.
[44] Yao DJ. In-plane MEMS thermoelectric microcooler, Ph.D. Dissertation, UCLA; 2001.